

MEASUREMENTS OF THE REACTION  
CROSS SECTIONS OF NEUTRON-RICH Sn ISOTOPES  
AT THE R<sup>3</sup>B SETUP\*

E. KUDAIBERGENOVA<sup>a,†</sup>, I. LIHTAR<sup>b</sup>, M. FEJOO-FONTÁN<sup>c</sup>  
T. AUMANN<sup>a,d,e</sup>, C.A. BERTULANI<sup>f</sup>, I. GAŠPARIĆ<sup>b</sup>, A. HORVAT<sup>a,b</sup>  
V. PANIN<sup>d</sup>, J.L. RODRÍGUEZ-SÁNCHEZ<sup>c,g</sup>, D. ROSSI<sup>a,d</sup>  
S. STORCK-DUTINE<sup>a</sup>, H.T. TÖRNQVIST<sup>d,h</sup>, H. ALVAREZ-POL<sup>c</sup>  
L. ATAR<sup>d</sup>, J. BENLLIURE<sup>c</sup>, K. BORETZKY<sup>d</sup>, L.T. BOTTI<sup>i</sup>, C. CAESAR<sup>d</sup>  
E. CASAREJOS<sup>j</sup>, J. CEDERKÄLL<sup>k</sup>, A. CHATILLON<sup>l</sup>, D. CORTINA-GIL<sup>c</sup>  
E. DE FILIPPO<sup>m</sup>, T. DICKEL<sup>d</sup>, M. DUER<sup>a</sup>, A. FALDUTO<sup>a</sup>  
L.M. FONSECA<sup>a</sup>, D. GALAVIZ<sup>n</sup>, G. GARCÍA-JIMÉNEZ<sup>c</sup>, Z. GE<sup>d</sup>  
E.I. GERACI<sup>o</sup>, R. GERNHÜSER<sup>p</sup>, B. GNOFFO<sup>o</sup>, A. GRAÑA-GONZÁLEZ<sup>c</sup>  
K. GÖBEL<sup>d</sup>, A.L. HARTIG<sup>a</sup>, M. HEIL<sup>d</sup>, A. HEINZ<sup>h</sup>, T. HENSEL<sup>q</sup>  
M. HOLL<sup>a,h</sup>, A. JEDELE<sup>a</sup>, D. JELAVIĆ-MALENICA<sup>b</sup>, T. JENEGGER<sup>p</sup>  
L. JI<sup>a</sup>, H.T. JOHANSSON<sup>h</sup>, B. JONSON<sup>h</sup>, N. KALANTAR-NAYESTANAKI<sup>r</sup>  
A. KELIĆ-HEIL<sup>d</sup>, O.A. KISELEV<sup>d</sup>, P. KLENZE<sup>d</sup>, D. KÖRPER<sup>d</sup>  
T. KRÖLL<sup>a</sup>, YU.A. LITVINOV<sup>d</sup>, B. LÖHER<sup>d</sup>, N.S. MARTORANA<sup>s</sup>  
P. MORFOUACE<sup>l</sup>, S. MURILLO-MORALES<sup>t</sup>, C. NOCIFORO<sup>d</sup>  
A. OBERTELLI<sup>a</sup>, S. PASCHALIS<sup>t</sup>, A. PEREA<sup>u</sup>, M. PETRI<sup>t</sup>, S. PIETRI<sup>d</sup>  
S. PIRRONE<sup>m</sup>, L. PONNATH<sup>p</sup>, H.B. RHEE<sup>a</sup>, L. ROSE<sup>t</sup>, P. RUSSOTTO<sup>s</sup>  
D. SAVRAN<sup>d</sup>, H. SCHEIT<sup>a</sup>, H. SIMON<sup>d</sup>, J.P. SIMON<sup>a</sup>, A.M. STOTT<sup>t</sup>  
Y. SUN<sup>a</sup>, D. SYMOCHKO<sup>a</sup>, C. SÜRDER<sup>a</sup>, J. TAIEB<sup>l</sup>, R. TANIUCHI<sup>t</sup>  
O. TENGBLAD<sup>u</sup>, S. VELARDITA<sup>a</sup>, F. WAMERS<sup>d</sup>

for the R<sup>3</sup>B Collaboration

*Received 10 November 2023, accepted 15 January 2024,  
published online 24 April 2024*

A fundamental framework to describe nuclear matter as a function of pressure and nuclear isospin asymmetry is the nuclear Equation of State (EoS). Constraining the parameters of the EoS is one of the central issues in nuclear physics, especially since the slope parameter  $L$  has not yet been constrained well experimentally. It has been identified that a precise determination of the neutron-removal cross section in neutron-rich nuclei, which correlates with the neutron-skin thickness, would provide a more precise constraint on  $L$ . To this end, an experiment was performed at the R<sup>3</sup>B setup in the GSI Helmholtzzentrum für Schwerionenforschung GmbH as a part of the FAIR Phase-0 program. The reactions are studied in inverse

\* Presented at the XXXVII Mazurian Lakes Conference on Physics, Piaski, Poland, 3–9 September, 2023.

† Affiliations listed at the end of the paper.

kinematics with neutron-rich tin isotopes in the mass range of  $A = 124\text{--}134$  on carbon targets of different thicknesses. The reaction products have been measured at beam energies of 400–900 MeV/ $u$  in a kinematically complete manner. In this communication, the analysis of  $^{124}\text{Sn} + ^{12}\text{C}$  at 900 MeV/ $u$  is presented. The charge-exchange reactions, resulting processes, and their role in the calculation of other reaction cross sections are discussed.

DOI:10.5506/APhysPolBSupp.17.3-A18

## 1. Introduction

The nuclear Equation of State (EoS) plays a key role in many different aspects of modern physics, being fundamental for understanding the structure of nuclear matter, the properties of neutron stars, and the synthesis of heavy elements. The nuclear EoS describes the energy per nucleon as a function of the density  $\rho$  and the relative proton–neutron asymmetry  $\delta = (N - Z)/(N + Z)$ . For asymmetric nuclear matter, the EoS depends on the symmetry energy  $S(\rho)$  with its value  $J$  and slope parameter  $L = 3\rho_0 \partial S(\rho)/\partial \rho|_{\rho=\rho_0}$  at saturation density  $\rho_0$ . The symmetry energy at saturation  $J$  is relatively well constrained experimentally [1]. However, the density-dependent parameter  $L$  is still poorly known.

It has been shown that the neutron-skin thickness of neutron-rich nuclei is a highly sensitive observable, providing more accurate constraints on the slope of the symmetry energy [2]. A close relation has been found between the total neutron-removal cross section  $\sigma_{\Delta N}$  and the neutron-skin thickness  $\Delta r_{np}$  as well [3]. This correlation enables a new approach to effectively constrain  $L$ . The new method, which is based on a precise measurement of the total neutron-removal cross section of neutron-rich nuclei, could provide a possible constraint on  $L$  with an accuracy  $\Delta L \approx 10$  MeV. In order to reach this, the measurement of  $\sigma_{\Delta N}$  has to be performed with 2% accuracy [3], which is the major goal of the experiment described in the next section.

In addition, one can measure the total reaction  $\sigma_R$  and the total charge-changing  $\sigma_{\Delta Z}$  cross sections in the same analysis. During the latter, events leading to a charge increase have been observed. These events are the result of the charge-exchange reactions, which should be considered as a component of the neutron-removal as will be discussed in Section 3.

## 2. Experiment

The experiment was carried out at the R<sup>3</sup>B (Reactions with Relativistic Radioactive Beams) setup at GSI in Darmstadt. It is a versatile setup with high efficiency and acceptance for the reaction measurements, which consists of the large-acceptance superconducting dipole magnet GLAD and several detection subsystems.

The setup of the performed experiment is shown in Fig. 1. The incoming ions are detected by a PSP (Position Sensitive Pin diode) detector. The target area is surrounded by the CALIFA (CALorimeter for In-Flight detection of gamma rays and high energy charged pArticles)  $\gamma$ -ray detector. The outgoing beam and fragment charges are measured by the R3B-MUSIC (MULTiple Sampling Ionisation Chamber) [5]. Evaporated neutrons are detected with NeuLAND (New Large Area Neutron Detector) [6] which is placed at  $0^\circ$  with respect to the beam axis at the end of the setup, while trajectories of charged particles are bent by  $18^\circ$  by the GLAD. Isotopes are tracked with  $x$  and  $y$  position information from a MWPC (Multi Wire Proportional Chamber) detector [7] in front of the magnet, and from FIBER detectors behind the magnet.

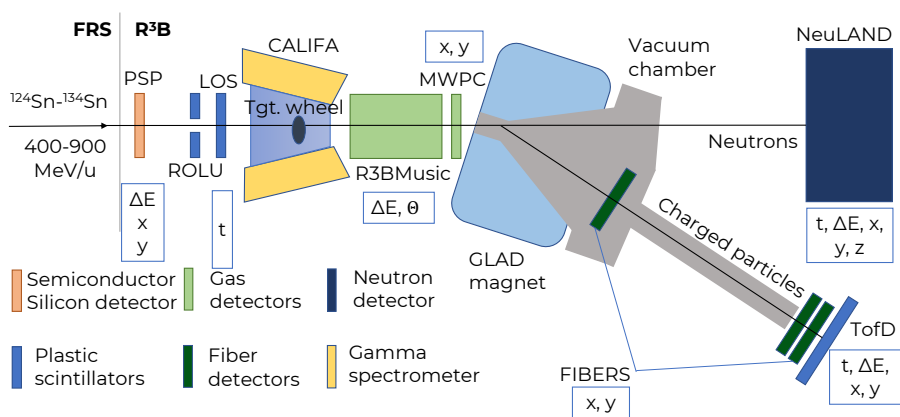


Fig. 1. A schematic drawing of the experimental setup. The incoming beam is identified event-by-event in charge and mass. Charged fragments are likewise identified using the detectors around the GLAD magnet. Outgoing neutrons are detected by the neutron detector NeuLAND in the forward direction.

Secondary cocktail beams were produced in the FRS (Fragment Reaction Separator) [8]. They were obtained from two different reaction mechanisms. The first is the fragmentation of the  $^{136}\text{Xe}$  primary beam at  $1.08\text{ GeV}/u$  and  $620\text{ MeV}/u$  using a Be target. The second is the  $^{238}\text{U}$  fission at  $1000\text{ MeV}/u$  and  $750\text{ MeV}/u$ , using a Pb target. As a result, cocktail beams centered on  $^{124}\text{Sn}$ ,  $^{132}\text{Sn}$ , and  $^{134}\text{Sn}$  isotopes with energies  $400\text{--}900\text{ MeV}/u$  were delivered to the experimental area. The secondary targets used in the experiment were C ( $1\text{ g}/\text{cm}^2$ ,  $2\text{ g}/\text{cm}^2$ ),  $\text{CH}_2$  ( $1\text{ g}/\text{cm}^2$ ,  $2\text{ g}/\text{cm}^2$ ), and Pb ( $980\text{ mg}/\text{cm}^2$ ).

### 3. Analysis and discussion

In this section, the analysis of the  $^{124}\text{Sn}+^{12}\text{C}$  reaction with a projectile energy of 900 MeV/ $u$  and target thickness of 1 g/cm $^2$  and 2 g/cm $^2$  is presented. Measurements with an empty target frame were used to estimate the background reaction contribution.

The incoming ions are identified with a charge ( $Z$ ) *versus* mass-over-charge ( $A/q$ ) plot, shown in Fig. 2, left.  $Z$  is measured by the PSP detector,  $A/q$  is proportional to  $B\rho/\beta\gamma$ , where the magnetic rigidity  $B\rho$  is known from the FRS setting, and velocity  $\beta\gamma$  is obtained by measuring ToF (Time-of-Flight) between the plastic scintillator at the S2 focal plane in the FRS and the LOS before the secondary target. An elliptical cut was used to select the isotope of interest. After the incoming beam identification, the outgoing charge spectra from the R3B-MUSIC detector, placed after the target wheel, are analyzed. Reaction products are measured in a charge range of  $Z = 26\text{--}54$  with resolution of  $\Delta Z/Z \approx 3 \times 10^{-3}$ , providing a good charge separation.

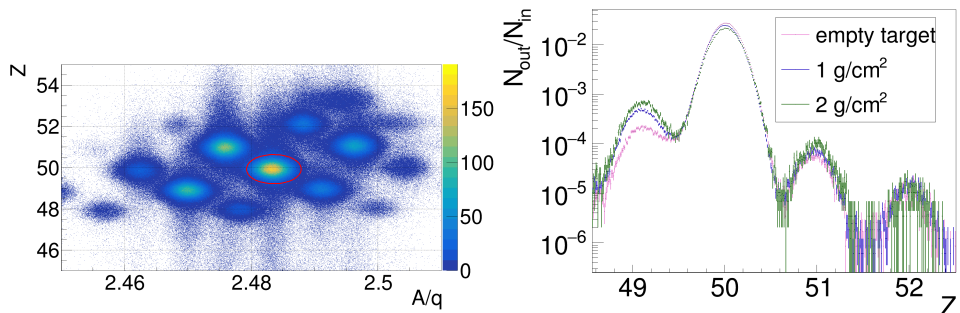


Fig. 2. (Colour on-line) Left: Incoming particle identification by  $Z$  and  $A/q$  measurements.  $^{124}\text{Sn}$  is indicated by a red/grey ellipse. Right: Comparison of outgoing particle counts in R3B-MUSIC ( $N_{\text{out}}$ ), normalized to the number of incoming particles ( $N_{\text{in}}$ ), for measurements with and without the target.

As mentioned in the introduction and shown in Fig. 2, right, a small number of events appearing at  $Z = 51$  are observed in the charge spectra, which result from the charge-exchange reactions. The background distribution at  $Z = 51$  is lower than the distributions of reaction products with the two different target thicknesses. An additional peak is also found around  $Z = 52$ . However, this is due to contamination, since there is no increase in the height of the  $Z = 52$  reaction peak compared to the data without a target. The presence of events with  $Z = 52$  inside the cut for  $Z = 50$  can be explained by the observation of asymmetric “tails” towards low energy-loss values detected by the PSP (Fig. 2, left). This allows a 0.07% of unreacted  $Z = 52$  events to be identified as  $Z = 50$  in the PSP, thus bypassing the incoming identification selection.

Concerning the  $\Delta Z = +1$  reaction, there are two possible processes resulting in an increase in the nuclear charge of the projectile at high-beam energies. One is the Gamow–Teller (GT) resonance, which is a collective nuclear excitation mode involving a spin–isospin flip of a nucleon [9]. The other one is the excitation of a  $\Delta(1232)$  resonance and its subsequent decay to a proton and a pion [10, 11]. The second contribution is significant for kinetic energies  $E_k \gtrsim 300$  MeV/ $u$  (the pion production threshold in the laboratory frame), while the GT resonance can be observed at the excitation energy  $E_{\text{ex}} \approx 16.5$  MeV [12].

The production of  $Z + 1$  nuclei via the  $\Delta$  resonance is considered in the reaction theory based on the Glauber model, while the collective excitations are not included [13], since the model treats nucleons as independent particles moving in the nuclear potential. In order to compare the experimentally obtained  $\sigma_{\Delta Z}$  and  $\sigma_{\Delta N}$  with the theoretically deduced cross sections, these two reaction processes need to be disentangled. One of the methods to reveal the presence of these two contributions is a comparison of kinetic energies of  $^{124}\text{Sn}$  and  $^{124}\text{Sb}$  fragments at the end of the experimental setup, which would allow to estimate the energy carried away by the pion [10].

The charge-changing cross section comprises all nuclear reactions in which the nuclear charge of the projectile changes. Events, in which at least one neutron is removed from the projectile with an unchanged charge number, belong to the neutron-removal channel of the reaction cross section. In the charge-exchange reaction that turns a neutron into a proton, the primary interaction between the projectile and the target occurs with a projectile neutron. This type of events, however, should not be considered when extracting charge radii from the  $\sigma_{\Delta Z}$ , since the primary reaction originates from the neutron of the projectile. Consequently, the charge-exchange cross section is calculated separately and needs to be added to the neutron-removal cross-section value, when extracting neutron radii.

#### 4. Conclusion

In this work, the observation of the  $Z + 1$  channel in the reaction of  $^{124}\text{Sn}$  with carbon targets at 900 MeV/ $u$  is discussed. Two reaction mechanisms resulting in charge increase at high-beam energies are described, namely the GT resonance and the  $\Delta$ -resonance. The analysis of  $Z + 1$  production is an intermediate step in order to obtain  $\sigma_{\Delta Z}$  and  $\sigma_{\Delta N}$  values more accurately. The cross sections of such charge-exchange reactions are necessary to derive the final neutron-removal cross section. Further work will include the investigation of charge-exchange reactions at lower-beam energies for  $^{124}\text{Sn}$  and for other tin isotopes.

The project was supported by the BMBF via Project No. 05P21RDFN2, the Helmholtz Research Academy Hessen for FAIR and the GSI-TU Darmstadt cooperation.

## REFERENCES

- [1] M. Tsang *et al.*, *Phys. Rev. C* **86**, 015803 (2012).
- [2] X. Roca-Maza, M. Centelles, X. Viñas, M. Warda, *Phys. Rev. Lett.* **106**, 252501 (2011).
- [3] T. Aumann, C.A. Bertulani, F. Schindler, S. Typel, *Phys. Rev. Lett.* **119**, 262501 (2017).
- [4] H. Alvarez-Pol *et al.*, *Nucl. Instrum. Methods Phys. Res. A* **767**, 453 (2014).
- [5] W. Christie *et al.*, *Nucl. Instrum. Methods Phys. Res. A* **255**, 466 (1987).
- [6] K. Boretzky *et al.*, *Nucl. Instrum. Methods Phys. Res. A* **1014**, 165701 (2021).
- [7] ALICE Collaboration, *J. Phys. G: Nucl. Part. Phys.* **30**, 1517 (2004).
- [8] H. Geissel, G. Münzenberg, K. Riisager, *Annu. Rev. Nucl. Part. Sci* **45**, 163 (1995).
- [9] A. Obertelli, H. Sagawa, «Modern Nuclear Physics: From Fundamentals to Frontiers», *Springer Singapore*, Singapore 2021.
- [10] J.L. Rodríguez-Sánchez *et al.*, *Phys. Rev. C* **106**, 014618 (2022).
- [11] A. Kelić *et al.*, *Phys. Rev. C* **70**, 064608 (2004).
- [12] J. Yasuda *et al.*, *Phys. Rev. Lett.* **121**, 132501 (2018).
- [13] E. Teixeira, T. Aumann, C. Bertulani, B. Carlson, *Eur. Phys. J. A* **58**, 205 (2022).

### List of affiliations:

<sup>a</sup>Technische Universität Darmstadt, Fachbereich Physik, 64289 Darmstadt, Germany

<sup>b</sup>RBI Zagreb, Bijenička cesta 54, HR10000, Zagreb, Croatia

<sup>c</sup>IGFAE, Universidade de Santiago de Compostela, 15782 Santiago de Compostela, Spain

<sup>d</sup>GSI Helmholtzzentrum für Schwerionenforschung, Planckstraße 1, 64291 Darmstadt, Germany

<sup>e</sup>Helmholtz Research Academy Hesse for FAIR, 64289 Darmstadt, Germany

<sup>f</sup>Texas A&M University-Commerce, 75428, Commerce, TX, USA

<sup>g</sup>CITENI, Campus Industrial de Ferrol, Universidade da Coruña, 15403 Ferrol, Spain

<sup>h</sup>Institutionen för Fysik, Chalmers Tekniska Högskola, 412 96 Göteborg, Sweden

<sup>i</sup>Goethe-Universität Frankfurt, Max-von-Laue Str. 1, 60438 Frankfurt am Main, Germany

<sup>j</sup>CINTECX, Universidade de Vigo, DSN, Dpt. Mech. Engineering, 36310 Vigo, Spain

<sup>k</sup>Lund University, Department of Physics, P.O. Box 118, 221 00, Lund, Sweden

<sup>l</sup>CEA, DAM, DIF, 91297 Arpajon, France

<sup>m</sup>INFN Sezione di Catania, Via Santa Sofia 64, 95123, Catania, Italy

<sup>n</sup>Laboratório de Instrumentação e Física Experimental de Partículas, LIP, Av. Prof. Gama Pinto 2, 1649-003 Lisbon, Portugal

<sup>o</sup>Università di Catania, Dipartimento di Fisica e Astronomia "Ettore Majorana", Catania, Italy

<sup>p</sup>Technische Universität München, James-Franck-Str. 1, 85748, Garching, Germany

<sup>q</sup>Helmholtz-Zentrum Dresden-Rossendorf, Institute of Radiation Physics, Bautzner Landstraße 400, 01328, Dresden, Germany

<sup>r</sup>ESRIG, University of Groningen, Groningen, The Netherlands

<sup>s</sup>INFN Laboratori Nazionali del Sud, Via Santa Sofia 62, 95123, Catania, Italy

<sup>t</sup>School of Physics, Engineering and Technology, University of York, YO10 5DD York, UK

<sup>u</sup>Instituto de Estructura de la Materia, CSIC, 28006 Madrid, Spain